Metals & corrosion

Influence of silicon addition on intercritical annealing process and tensile properties of medium Mn steel

Yan Li[1], Runxun Wang[2], Baofeng Wang[2], and Wei Ding[2,*]

[1] *Bayan Obo Multi-Metallic Resource Comprehensive Utilization Key Laboratory, Inner Mongolia University of Science and Technology, Baotou 014010, People's Republic of China*

[2] *School of Material and Metallurgy, Inner Mongolia University of Science and Technology, Baotou 014010, People's Republic of China*

ABSTRACT

This paper presents research on the equilibrium phase fractions, microstructure, and tensile properties of a 0.2C–5Mn–1.5Al (mass %) steel with 0 or 0.5 (mass %) Si addition after intercritical annealing (IA), using thermodynamic simulation, scanning electron microscopy, transmission electron microscopy, X-ray diffractometry, and uniaxial tensile testing. The research results show that the addition of 0.5 Si (mass %) has no significant effect on the equilibrium phase fraction but influences the optimal IA temperature. Different IA temperatures result in the retained austenite having different morphologies. The retained austenite in the 730 °C sample (0.5 Si) has two different morphologies—polygonal and lath—while the 760 °C sample (0 Si) has only polygonal retained austenite. The optimal tensile properties of the 0.5 Si steel are better than those of the 0 Si steel due to the solution strengthening effect of Si and the higher stability of retained austenite. The tensile properties of the investigated 0.5 Si steel are excellent, with a tensile strength of over 1 GPa, elongation over 42.00%, and strength × ductility over 42 GPa%.

Introduction

In the past several decades, advanced high-strength steels (AHSS) have been widely applied in the automobile industry to meet the body-in-white weight reduction strategies pursued globally by car manufacturers for fuel economy and vehicle safety [1, 2].

AHSS have developed from the first generation to the third generation [3, 4], which have mechanical properties that exceed those of the first-generation AHSS and a potentially lower cost than that of the second-generation AHSS.

Medium Mn steels with a manganese content of 3–12 (mass %) are considered a powerful candidate material for third-generation AHSS and have been

extensively investigated [5–13]. Transformation from austenite to martensite during tensile deformation, that is, transformation-induced plasticity (TRIP), is one of the prominent strategies used to obtain the desired tensile properties for the medium Mn TRIP steel [14, 15]; therefore, the fraction and stability of the austenite are very important. The Fe–C–Mn medium Mn steels, with increased content of Mn compared with the first-generation AHSS, effectively stabilize austenite and increase the retained austenite fraction [8, 16, 17].

The intercritical annealing (IA) process is used to get the needed microstructure. During IA, carbon and manganese partition from α- or α′-martensite to austenite, and a long IA time are often required because of the slow diffusion of manganese [17, 18]. Recently, to shorten the IA time, Al was added to Fe–C–Mn medium Mn steel, because Al can increase the IA temperature, which shortens the time needed [10]. Moreover, Al can enlarge the austenite–ferrite two-phase range, and this increased range expands the processing window [19]. More interestingly, the twinning induced plasticity (TWIP) effect [7, 9] and δ-ferrite [20, 21] were observed in medium Mn TRIP steel when the Al content was higher than 2.5%, which further improved the mechanical properties of the steel.

But, the addition of Al introduces some problems, such as alumina inclusion and a decreased rate of continuous casting [22]. Therefore, the content of Al should be limited to a suitable range. Research has shown that the addition of Al in first-generation AHSS as an alloying element partially or completely replaced Si, and that the content of Al was no more than 1.5% (mass %) [23–25].

For TRIP steels, one of the first-generation AHSS, Si, is a very important alloying element because it is an effective solid solution strengthening element [26] and it can inhibit carbide precipitation [27]. The previous research in low Mn and high Mn steels [27–29] suggests that Si is also a useful alloying element in medium Mn steels. However, related information on TRIP and dual-phase steels is not helpful [30] because of the different roles of Si in these various AHSS and the different scales of the microstructure. It is thus worthwhile to investigate the effect of Si on the overall mechanical behavior of medium Mn steels to facilitate alloy design.

The present work investigates the influence of Si on the equilibrium phase fraction, IA process, microstructure, and mechanical properties of 0.2C–5Mn–1.5Al–xSi (x = 0 or 0.5) medium Mn steels. The microstructure evolution process and stress–strain behavior of medium Mn steels under different Si alloy conditions are studied in detail. The influence of Si on the microstructure and mechanical properties of this steel is comparatively analyzed.

Materials and methods

Table 1 shows the nominal composition of the investigated medium Mn steels with different Si additions, which is also used in CALPHAD calculations. The steels are referred to as 0 Si and 0.5 Si in this study for convenience. The ingot of medium Mn steel was cast using a vacuum induction furnace (the composition of ingot is also shown in Table 1). The steel ingots were reheated to 1200 °C for 60 min and hot-rolled to 3.5 mm above 950 °C, maintained at 600 °C for 1.5 h, and subsequently furnace cooled to room temperature for coiling simulation. The coiling simulation is to make the microstructure of hot-rolled plates in this paper as close as possible to the microstructure of industrial products. After surface descaling, the hot-rolled plates were cold-rolled to 1.4-mm-thick sheets (60% reduction) at room temperature. Using the FactSage®7.3 software and FSstel databases, the transformation temperatures—A_1, A_{CM}, and A_3—were calculated as 490.5, 655, and 847.7 °C, respectively, for the 0 Si, and also, 493, 660.5, and 871 °C, respectively, for the 0.5 Si. Thereafter, specimens were intercritically annealed in a salt bath for 3 min at 700, 730, 760, or 790 °C, as schematically illustrated in Fig. 1.

The microstructures of the specimens were investigated using scanning electron microscopy (SEM; ZEISS-GeminiSEM 300) and transmission electron microscopy (TEM; JEOL F200) operated at 200 kV. The sample for SEM was mechanically ground and subsequently electro-polished with 85 vol% CH_3COOH and 15 vol% $HClO_4$ solution. Thin foil

Table 1 Composition of the two investigated steels (mass %)

Alloy	C	Mn	Al	Si	Fe
0 Si	0.2 (0.19)	5 (5.25)	1.5 (1.56)	0 (< 0.05)	Bal
0.5 Si	0.2 (0.19)	5 (5.35)	1.5 (1.60)	0.5 (0.51)	Bal

Figure 1 A schematic illustration of the steel preparation process. The ingot was hot-rolled, cooled, and then cold-rolled. Specimens were cut from the cold-rolled sheet and annealed at one of four temperatures for 3 min before air cooling.
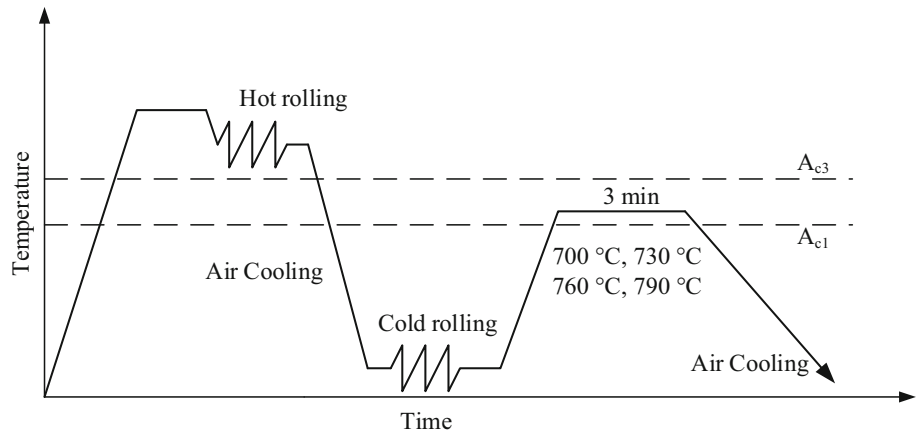
specimens for TEM were mechanically ground to 50 μm in thickness and punched to round disks (φ3 mm), followed by electro-polishing at − 20 °C in a twin-jet polisher using a solution of 95 vol% CH_3-COOH and 5 vol% $HClO_4$.

Retained austenite fractions were quantified by X-ray diffraction (XRD; Bruker D8 ADVANCE) using Cu Ka radiation with a scan step size of 0.02, and a 2θ scan range from 40 to 100° was employed. Specimens for XRD were mechanically polished and subsequently electro-polished at 15 V at room temperature in a solution of 20 vol% $HClO_4$ and 80 vol% CH_3-COOH. The integrated intensity (I) of the $(200)_\alpha$ and $(211)_\alpha$ peaks and the $(200)_\gamma$, $(220)_\gamma$, and $(311)_\gamma$ peaks was determined using least-square fitting of a Pearson VII-type function, and the volume fraction of retained austenite (V_γ) was calculated using the direct comparison method according to Cullity and Stock [31] as follows:

$$V_\gamma = \left[\frac{1}{q}\sum_{j=1}^{q}\frac{I_{\gamma j}}{R_{\gamma j}}\right] / \left[\frac{1}{q}\sum_{j=1}^{q}\frac{I_{\gamma j}}{R_{\gamma j}} + \frac{1}{p}\sum_{i=1}^{p}\frac{I_{\alpha i}}{R_{\alpha i}}\right] \times 100\%, \quad (1)$$

where R and I are the calculated theoretical and experimental intensity for a certain peak, respectively, q is the number of austenite peaks, and p is the number of ferrite/martensite peaks.

The dog-bone-shaped tensile specimens were machined along the rolling direction with a gauge length of 25 mm according to the ASTM-E8 standard. Uniaxial tensile tests were carried out at room temperature for the selected annealed specimens in a CMT universal testing machine with a load range of 300 kN. The crosshead speed was maintained at 2 mm min^{-1}. Two specimens were tested for each heat treatment.

Modeling

The change of chemical composition in medium Mn steel will have a certain effect on the phase transformation in the IA process. To predict the composition and phase fraction of each phase in the annealed specimen, a retained austenite prediction model assuming ortho-equilibrium alloy partitioning at IA temperatures was used [32]. Equilibrium fractions of austenite, ferrite, and cementite and their chemical compositions as a function of the IA temperature for the two alloy steels were calculated using FactSage 7.3 software and databases. The fraction of fresh martensite transformed during cooling was then calculated by the Johnson–Mehl–Avrami–Kolmogorov (JMAK) equation [33]:

$$f_M = f_\gamma[1 - \exp\{-0.011(M_s - RT)\}], \quad (2)$$

where f_M is the phase fraction of fresh martensite transformed during cooling, f_γ is the fraction of reverse austenite, RT is room temperature (25 °C), and M_S is the starting temperature of martensitic transformation, calculated by the modified Andrew equation [32, 34]:

$$M_s \ (°C) = 539 - 423C - 30.4Mn - 7.5Si + 30Al. \quad (3)$$

Finally, the content of retained austenite ($f_{\gamma R}$) after annealing at each IA temperature was obtained by the subtraction of f_M from f_γ.

The degree of strain-induced martensite transformation during tensile deformation was estimated using the chemical composition of retained austenite. For a simple fitting of the martensite transformation kinetics, the Sugimoto equation with a single K_S related to austenite stability was selected, and the
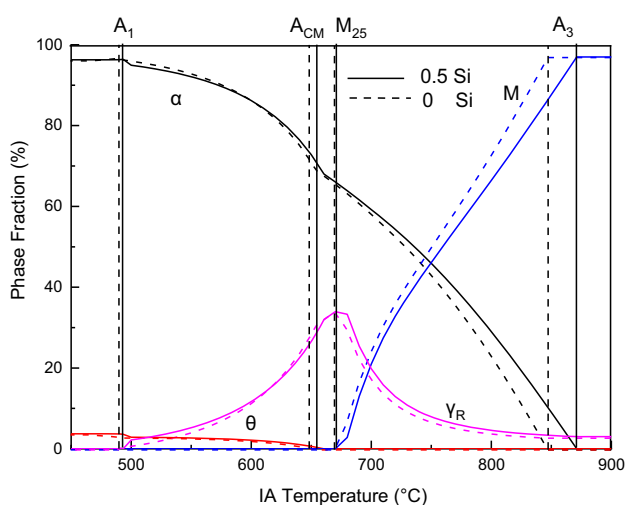
relationship between the K_S parameter and M_S was determined [35]:

$$K_S = 3.06 \exp(M_s/79.7) - 1.39. \qquad (4)$$

Results and discussion

Influence of Si on equilibrium phase fractions

Figure 2 shows the equilibrium phase fractions in the 0 Si and 0.5 Si steels at room temperature after IA, using FactSage 7.3 software and steel databases, and Eqs. (2) and (3). The ferrite, retained austenite, martensite, and cementite are expressed as α, γ_R, M, and θ, respectively. Four vertical lines represent the four phase transition temperatures of the sample during the experiment: austenitization starting temperature during heating (A_1); austenitization finishing temperature during heating (A_3); cementite complete dissolution temperature during heating (A_{CM}); and an IA temperature where the Ms of the intercritical austenite equals room temperature (25 °C) due to solute partitioning (M_{25}) [32, 36]. The figure shows that the addition of Si influences the A_3 temperature of the test steel; the A_3 temperature increases from 847.7 °C for the 0 Si to 871 °C for the 0.5 Si. But the addition of Si has only a slight effect on the A_1, A_{CM}, and M_{25} of the test steel. The
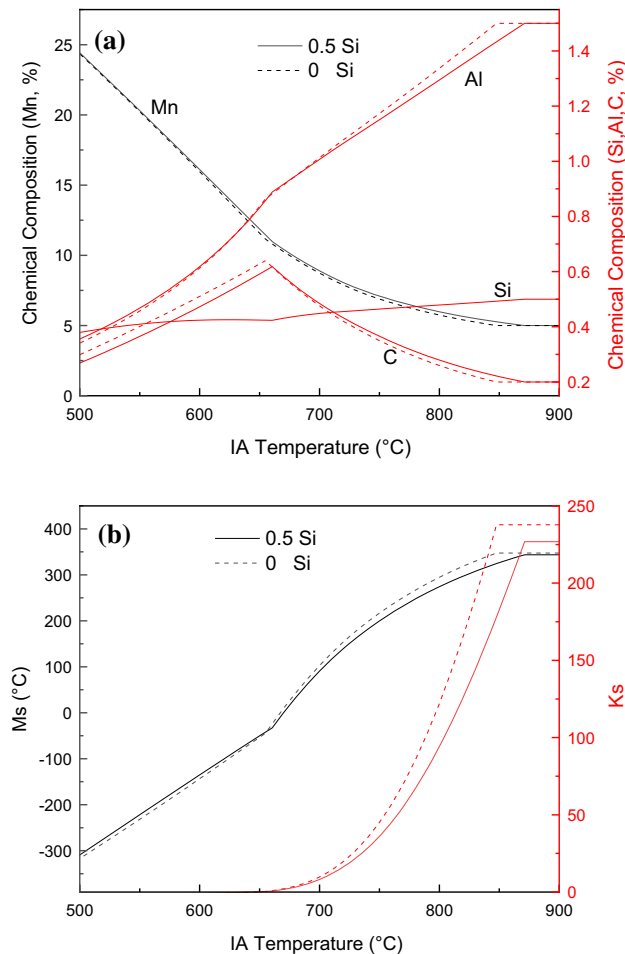
temperature of A_1 increases from 490.5 °C for the 0 Si to 493 °C for the 0.5 Si, A_{CM} increases from 655 to 660.5 °C, and M_{25} has almost no change, with both temperatures at 670 °C.

With increasing annealing temperature, the retained austenite fraction in the 0 Si and 0.5 Si steels shows a typical increase to a maximum value, followed by a decrease due to martensite formation upon cooling. When the steel intercritical annealing at a temperature higher than M_{25} temperature, the stability of intercritical austenite is insufficient; thus, some intercritical austenite will transform to martensite during cooling. Maximum value of austenite appears at the M_{25} temperature; 0 Si and 0.5 Si steels have similar maximum austenite contents. The intercritical austenite is fully stabilized by solute partitioning at temperatures below M_{25}, and no martensite is present below M_{25}. Ferrite and cementite are present below the intercritical temperatures of A_3 and A_{CM}, respectively. Due to the inhibition of Si on cementite precipitation, the maximum cementite content in 0 Si is slightly less than that in 0.5 Si.

To estimate the mechanical stability of retained austenite in the two steels, M_S temperatures and K_S values were calculated using Eqs. (3) and (4), based on the predicted chemical composition at each annealing temperature, as shown in Fig. 3. Over the entire IA temperature range, the M_S temperatures of the two alloys gradually increase with increasing annealing temperature. When the IA temperature is higher than 655 °C (A_{CM} temperature of 0 Si), the M_S temperature of 0 Si is slightly higher than that of 0.5 Si. The increased austenite stability results from the enrichment of C and Mn and the addition of Si. It is speculated that more martensite exists in 0 Si at higher critical annealing temperatures. Similar to the M_S temperature, the K_S value increases with the increase in annealing temperature. The K_S value of 0.5 Si steel is smaller than the K_s value of 0 Si steel, and the difference gradually increases with the increase in annealing temperature. A lower K_S value means less strain deformation of the martensite. In other words, the retained austenite in 0.5 Si steel has more difficulty undergoing martensitic transformation during the deformation process, so that the TRIP effect continues to occur. It is speculated that compared with 0 Si steel, 0.5 Si steel has better comprehensive mechanical properties.

Figure 2 Calculated phase fractions of ferrite (α), retained austenite (γ_R), cementite (θ), and martensite (M) for the 0 Si and 0.5 Si steels annealed in the intercritical temperature range using the FactSage®7.3 software and FSstel databases.

Figure 3 a Predicted chemical composition of austenite in the 0 Si and 0.5 Si steels after IA, and **b** predicted M_S temperatures and K_S values of austenite in the 0 Si and 0.5 Si steels after IA.

Microstructure

Figure 4 shows the microstructure of the test steel after IA, where (a), (c), (e), and (g) show the microstructure of 0 Si steel, and (b), (d), (f), and (h) show the microstructure of 0.5 Si steel. Table 2 shows the phase fractions of investigated steels with different IA temperatures. The figure shows that the microstructure of 0 Si and 0.5 Si alloys annealed at different temperatures contains a certain amount of ferrite (F) and a part of the retained austenite (RA). White grains appear in the samples annealed at relatively low temperatures, which are presumed to be cementite (θ). With the increase in annealing temperature, another phase is introduced, which is fresh martensite (M) transformed from reverse austenite during cooling, and the content of retained austenite begins to decrease. The main reason for this

phenomenon is that as the temperature increases, the reversed austenite grains grow, and the C and Mn in the reversed austenite are insufficient to maintain the reversed austenite's stability; martensitic transformation occurs in the subsequent cooling process, so the martensite begins to appear and the retained austenite decreases. Comparing the microstructures of 0 Si and 0.5 Si, the content of cementite in 0.5 Si steel is significantly lower than that in 0 Si steel at lower temperatures. When the annealing temperature reaches 730 °C, there is no cementite in 0.5 Si steel, and the cementite in 0 Si steel disappears completely during 760 °C annealing, because Si can inhibit the precipitation of cementite [27]. The figure shows that martensite appears in 0.5 Si at 760 °C, while martensite begins to appear at 790 °C in 0 Si, results that relate to the stability of reverse austenite in the IA process.

TEM observation was used to study the retained austenite morphology in more detail. The retained austenite of the 730 °C sample (0.5 Si) is shown in Fig. 5a, and the retained austenite of the 760 °C sample (0 Si) is shown in Fig. 5b, c.

The diffraction patterns in Fig. 5a1, a2 show that the phase of the polygonal and lath morphologies, marked with red circles in Fig. 5a, is retained austenite, and the zone axis of both different morphologies of retained austenite is parallel to the beam. There are two different morphologies of retained austenite in the 730 °C sample; part of the retained austenite is marked using red arrows in Fig. 5a. One morphology, polygonal retained austenite, has a grain size of about 300–500 nm in diameter. The other, lath retained austenite, has a grain size of about 100 nm in lath width.

The diffraction pattern in Fig. 5b1 shows that the phase of the polygonal morphology marked with red circles in Fig. 5b is retained austenite. Figure 5b2 is the dark-field image of the red rectangle in Fig. 5b1; all the bright regions in Fig. 5b2 are retained austenite (marked using red arrows). Figure 5c is also the dark-field image of the red rectangle in Fig. 5b1 and has a larger view field than the image in Fig. 5b2. Figure 5c shows that there is only one morphology, the polygonal morphology, of retained austenite in the 760 °C sample. The grain size of retained austenite shown in Fig. 5c is about 300–800 nm in diameter, which means that the retained austenite grain size of the 760 °C sample is coarser than that of the 730 °C sample.
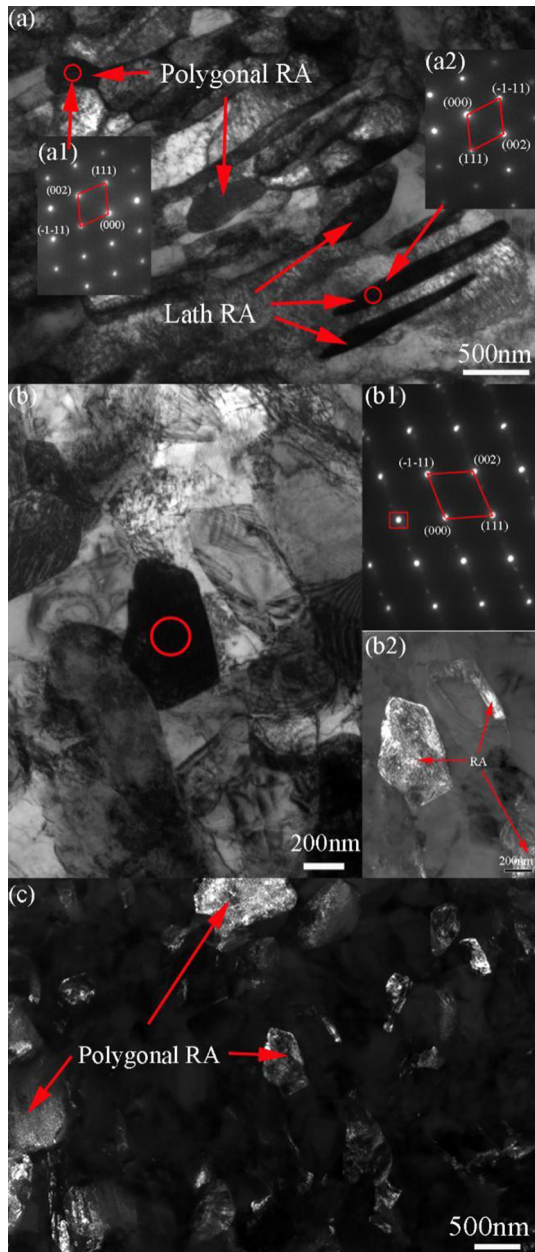
Figure 4 SEM micrographs of investigated samples intercritically annealed at different temperatures. The IA temperatures are as follows: **a**, **b** 700 °C; **c**, **d** 730 °C; **e**, **f** 760 °C; and **g**, **h** 790 °C. Panels **a**, **c**, **e**, and **g** show the microstructure of 0 Si steel, and **b**, **d**, **f**, and **h** show the microstructure of 0.5 Si steel.
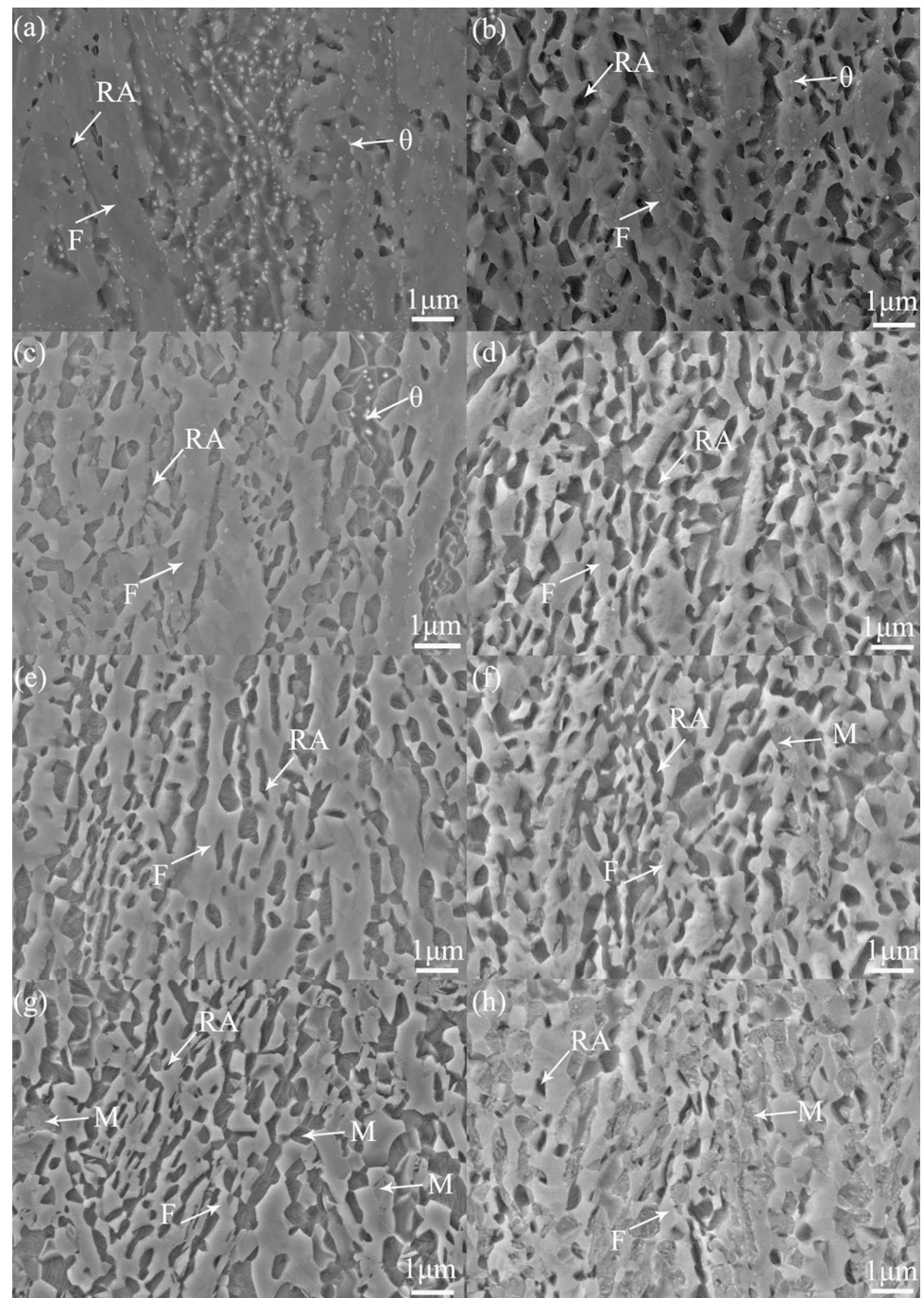
Table 2 Phase fractions of investigated steels with different IA temperatures (vol%)

	θ		F		RA		M	
	0 Si	0.5 Si	0 Si	0.5 Si	0 Si	0.5 Si	0 Si	0.5 Si
700 °C	5.06	3.02	78.96	86.37	15.98	10.61	0	0
730 °C	0.57	0	73.09	70.82	26.34	29.18	0	0
760 °C	0	0	69.17	53.49	30.83	26.34	0	20.17
790 °C	0	0	50.38	42.43	2.26	15.90	47.36	41.67

the 760 °C sample due to the smaller grain size and the lath morphology. The 730 °C sample is expected to have better mechanical properties than the 760 °C sample, especially the elongation, if there is no significant difference in the retained austenite fraction.

To visually show the change of retained austenite in the microstructures of the 0 Si and 0.5 Si steels, the samples after IA were studied by XRD. The volume fractions of retained austenite were calculated according to Eq. (1) and are shown in Fig. 6. The figure shows that with the increase in temperature, the retained austenite fraction in the 0 Si and 0.5 Si steels shows a typical increase to a maximum value, followed by a decrease due to martensite formation upon cooling; they reach the maximum value at 730 °C and 760 °C, respectively. This is due to the decrease in austenite stability with the increase in IA temperature, and the martensitic transformation that occurs in the subsequent cooling process. Compared with 0 Si steel, the maximum value of retained austenite in 0.5 Si steel shifted to the left (i.e., lower temperature in Fig. 6). It is speculated that Si can inhibit the precipitation of cementite, and the C and Mn elements are more likely to gather in austenite. In the experiment, the phase transformation is more likely to occur during annealing, to shift the phase transition process to the left, so that the maximum content of retained austenite in 0.5 Si steel can be obtained at a lower temperature. Figure 6 also shows a significant decrease in the retained austenite

Figure 5 TEM micrographs of the investigated samples. **a** Bright-field image of 730 °C sample (0.5 Si); **b** bright-field image of 760 °C sample (0 Si); and **c** dark-field image of 760 °C sample (0 Si).

As we know, the stability of the retained austenite is affected not only by the chemical composition, but also by the grain size and morphology [37, 38]: the smaller the retained austenite grain size, the better the stability [39]; and the stability of the lath morphology is better than that of the polygonal morphology [40]. Therefore, the stability of retained austenite in the 730 °C sample is better than that in
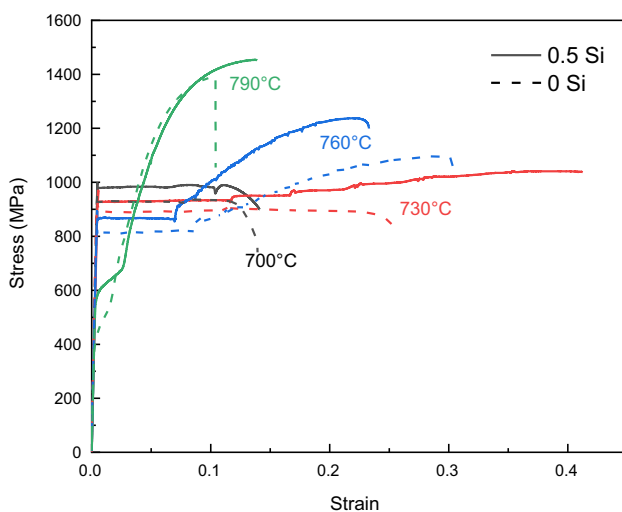

Figure 6 Retained austenite fraction of the investigated steels annealed at temperatures ranging from 700 to 790 °C for 3 min followed by cooling, and retained austenite fraction after tensile test of the investigated steels annealed at 730 and 760 °C for 3 min.

fraction after tensile test of 0 Si and 0.5 Si steels annealed at 730 and 760 °C. Retained austenite transforms into martensite due to the strain during the tensile deformation, thus shows the TRIP effect.
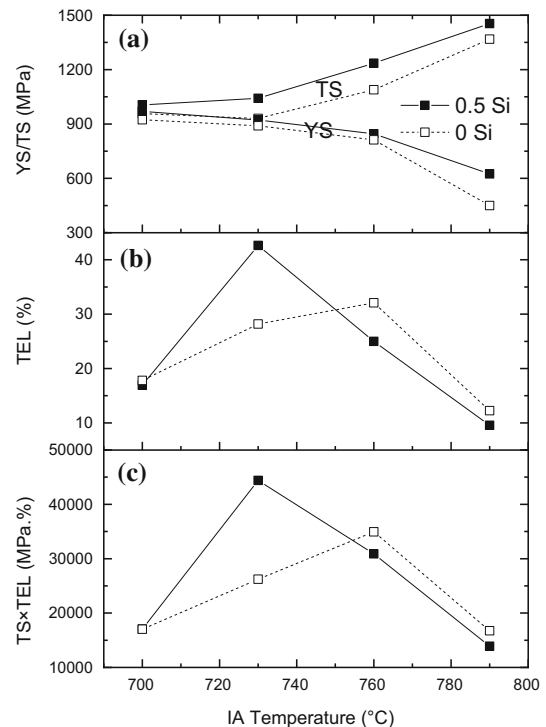
Mechanical properties

Figure 7 shows the measured room temperature stress–strain curves of 0 Si and 0.5 Si steels annealed for 3 min at 700–790 °C. The figure shows that the tensile deformation characteristics of the two steels are strongly affected by the annealing temperature. For example, the total elongation (TEL) of 0.5 Si steel annealed at 700 °C is 16.96%, while the TEL of the sample annealed at 730 °C is greatly increased, to 42.64%. In addition, the maximum tensile strength (TS) value of 1301 MPa obtained at 790 °C is 296 MPa higher than that at 700 °C. As expected, the 0.5 Si steel annealed at 730 °C, which had a higher $f_{\gamma R}$ value, exhibited a relatively larger TEL, and a greater TS was observed in the samples annealed above 730 °C, which had higher martensite fractions.

Figure 8 shows the TS, yield strength (YS), TEL, and TS × TEL as a function of annealing temperature for the 0 Si and 0.5 Si steels. Figure 8a shows the trends of the strength (YS and TS) of the test steel with the IA temperature. The figure shows that with an increase in IA temperature, the TS value of 0 Si initially decreases, reaches the minimum value at 730 °C, and then increases sharply at higher temperatures. However, the TS of 0.5 Si increases

Figure 8 Mechanical properties of the steels: **a** YS and TS, **b** TEL, and **c** TS × TEL of the 0 Si and 0.5 Si steels annealed at temperatures ranging from 700 to 790 °C for 3 min followed by cooling.

continuously with increasing IA temperature. The reason for the difference is that adding Si moves the conversion process to the left and eliminates the impact of recovery on the TS. The YS decreased with the increase of IA temperature. The YS values of 0 Si and 0.5 Si decrease with increasing IA temperature due to the degree of grain recovery and/or recrystallization, the formation of martensite, and the stability of retained austenite [41, 42]. With an increase in the IA temperature, the grain grows and the dislocation density decreases, which is also beneficial to dislocation slip and YS decrease. Continuous increase in the IA temperature will result in the formation of martensite during cooling. The martensite formation is associated with a volume dilatation, which results in the generation of internal compressive stresses in the regions surrounding the martensite islands. These stresses can act as back-stresses and lead to a reduction of the YS. Additionally, as the IA temperature increases, the yielding of those some unstable retained austenite is initiated by stress-induced transformation. The combination of the internal compressive stresses and the stress-induced

Figure 7 Room temperature stress–strain curves of the 0 Si and 0.5 Si steels annealed at temperatures ranging from 700 to 790 °C for 3 min followed by cooling.

transformation contributes to the substantial reduction of the YS. The figure also shows that the strength of 0.5 Si steel is generally higher than that of 0 Si steel due to the solution strengthening effect of Si.

In Fig. 8b, the TEL values of 0 Si and 0.5 Si steels show a peak value that changes with annealing temperature. The addition of Si increased the maximum TEL value from 32.08 to 42.64% and moved the peak to a lower temperature. This result is mainly related to the stability of retained austenite [32]. To some extent, TS × TEL can characterize the comprehensive mechanical properties of the material. As shown in Fig. 8c, with the increase in IA temperature, the TS × TEL values of the test steels increased first and then decreased. However, the maximum TS × TEL value obtained, at 730 °C for 0.5 Si steel, is significantly greater than that obtained, at 760 °C, for 0 Si steel. Compared with 0 Si steel, 0.5 Si steel can have more excellent comprehensive mechanical properties.

The work-hardening behavior of 0 Si steel at 760 °C (0 Si-760) and 0.5 Si steel at 730 °C (0.5 Si-730) is shown in Fig. 9. Before the necking, both samples have three distinct stages for work hardening that can be identified. Stage I is easily identified by the drastic decrease in the work-hardening rate and is commonly present in almost any steel independent of its microstructures [2]. This stage can be attributed to the easy glide of dislocations in a single system, because if each mobile dislocation could pass through the crystal without any barrier, the work-hardening rate would be exactly zero [43]. Stage II shows rapidly increasing work hardening for both samples. The emission of dislocations interacts with the gliding of

other dislocations [44], and cross-slip can occur [45], which increases the work hardening. However, this is not the only contribution to the increase in the work hardening. The dynamic transformation during deformation, from austenite to martensite (the TRIP effect), also produces an increase in the work-hardening during stage II.

In stage III, different work-hardening behaviors are seen for the two samples. The 0 Si-760 sample shows a decrease in the work-hardening rate due to the dislocation annihilation rate being greater than the dislocation multiplication rate induced by the TRIP effect and/or gliding dislocations. However, the work-hardening rate of the 0.5 Si-730 sample shows a jerk flow feature. The TRIP effect of retained austenite can produce an increase in the work hardening that to a certain degree offsets the decrease in work hardening due to dislocation annihilation. The 0.5 Si-730 sample has a diversity of retained-austenite stability because of its two different retained austenite morphologies; therefore, the TRIP effect exists at different stages of deformation and contributes to the work-hardening rate.

Conclusions

This paper presents research on the influence of 0.5 Si (mass %) on the IA process, microstructure, and tensile properties of 0.2C–5Mn–1.5Al (mass %) steels. The following conclusions can be drawn.

(1) The addition of 0.5 Si (mass %) has no significant effect on the equilibrium phase diagram, but influences the optimal IA temperature. The optimal IA temperature of 0 Si steel and 0.5 Si steel is 760 °C and 730 °C, respectively. The optimal IA temperature means that IA at this temperature produces the steel with the highest retained austenite fraction and optimal tensile properties.

(2) The different IA temperatures result in retained austenite with different morphologies. The 730 °C sample (0.5 Si) has two different retained austenite morphologies, polygonal and lath, while the 760 °C sample (0 Si) has only polygonal retained austenite. Therefore, the retained austenite of the 730 °C sample (0.5 Si) has better stability.

(3) The optimal tensile properties of the 0.5 Si steel are better than those of the 0 Si steel due to the solution strengthening effect of Si and the higher stability of retained austenite. The tensile properties
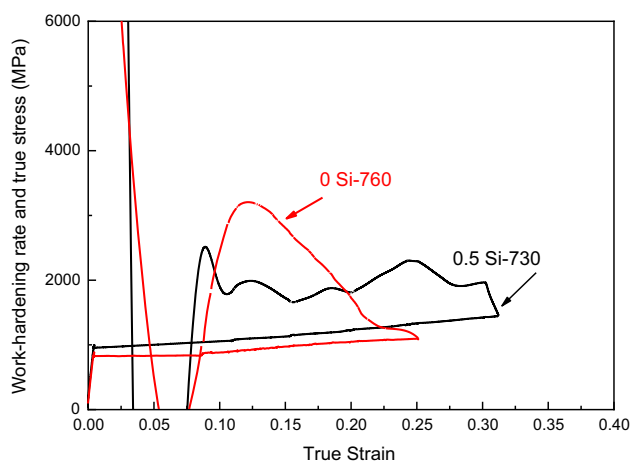
Figure 9 Work-hardening rate ($d\sigma/d\varepsilon$) and true stress–strain curves in 0 Si steel at 760 °C and 0.5 Si steel at 730 °C.

of the investigated 0.5 Si steels are excellent, with a tensile strength over 1 GPa, elongation over 42.00%, and strength × ductility over 42 GPa%.

Acknowledgements

Compliance with ethical standards

Conflict of interest The authors declare that they have no conflict of interest.

References

[1] Zhao J, Jiang Z (2018) Thermomechanical processing of advanced high strength steels. Prog Mater Sci 94:174–242. https://doi.org/10.1016/j.pmatsci.2018.01.006

[2] Zambrano OA (2018) Review A general perspective of Fe–Mn–Al–C steels. J Mater Sci 53:14003–14062. https://doi.org/10.1007/s10853-018-2551-6

[3] Li Y, Huyan F, Ding W (2019) Microstructure and tensile properties of a 0.20C–4.86Mn steel after short intercritical-annealing times. Mater Sci Technol 35:220–230. https://doi.org/10.1080/02670836.2018.1550864

[4] Matlock DK, Speer JG (2009) Third generation of AHSS: microstructure design concepts. In: Microstructure and texture in steels. Springer, pp 185–205

[5] Wang J, Hui W, Xie Z et al (2020) Influence of pre-strain on microstructural characteristics and tensile deformation behaviour of a cold-rolled Al-containing medium Mn steel. J Mater Sci 55:5296–5310. https://doi.org/10.1007/s10853-019-04337-3

[6] Aydin H, Essadiqi E, Jung IH, Yue S (2013) Development of 3rd generation AHSS with medium Mn content alloying compositions. Mater Sci Eng A 564:501–508. https://doi.org/10.1016/j.msea.2012.11.113

[7] Lee S, De Cooman BC (2014) Annealing temperature dependence of the tensile behavior of 10 pct Mn multi-phase TWIP-TRIP steel. Metall Mater Trans A 45:6039–6052

[8] Gibbs PJ, Moor EDE, Merwin MJ et al (2011) Austenite stability effects on tensile behavior of manganese-enriched-austenite transformation-induced plasticity steel. Metall Mater Trans A 42:3691–3702. https://doi.org/10.1007/s11661-011-0687-y

[9] Latypov MI, Shin S, De Cooman BC, Kim HS (2016) Micromechanical finite element analysis of strain partitioning in multiphase medium manganese TWIP+ TRIP steel. Acta Mater 108:219–228

[10] Lee YK, Han J (2015) Current opinion in medium manganese steel. Mater Sci Technol 31:843–856. https://doi.org/10.1179/1743284714Y.0000000722

[11] Hu B, Luo H, Yang F, Dong H (2017) Recent progress in medium-Mn steels made with new designing strategies, a review. J Mater Sci Technol 33:1457–1464. https://doi.org/10.1016/j.jmst.2017.06.017

[12] Suh D, Kim S (2017) Medium Mn transformation-induced plasticity steels: recent progress and challenges. Scr Mater 126:63–67. https://doi.org/10.1016/j.scriptamat.2016.07.013

[13] Perlade A, Antoni A, Besson R et al (2019) Development of 3rd generation medium Mn duplex steels for automotive applications. Mater Sci Technol 35:204–219. https://doi.org/10.1080/02670836.2018.1549303

[14] Ding R, Dai Z, Huang M et al (2018) Effect of pre-existed austenite on austenite reversion and mechanical behavior of an Fe–0.2C–8Mn–2Al medium Mn steel. Acta Mater 147:59–69. https://doi.org/10.1016/j.actamat.2018.01.009

[15] Lee H, Jo MC, Sohn SS et al (2018) Novel medium-Mn (austenite + martensite) duplex hot-rolled steel achieving 1.6 GPa strength with 20 % ductility by Mn-segregation-induced TRIP mechanism. Acta Mater 147:247–260. https://doi.org/10.1016/j.actamat.2018.01.033

[16] Lee S, De Cooman BC (2013) On the selection of the optimal intercritical annealing temperature for medium Mn TRIP steel. Metall Mater Trans A 44:5018–5024. https://doi.org/10.1007/s11661-013-1860-2

[17] Luo H, Shi J, Wang C et al (2011) Experimental and numerical analysis on formation of stable austenite during the intercritical annealing of 5Mn steel. Acta Mater 59:4002–4014. https://doi.org/10.1016/j.actamat.2011.03.025

[18] Ding W, Du J, Li Y (2020) Transformations during intercritical annealing and their implications for microstructure and mechanical properties of medium Mn transformation-induced plasticity steel in continuous annealing line. J Mater Eng Perform 29:23–31. https://doi.org/10.1007/s11665-019-04549-3

[19] Jiang H, Ding W, Tang D, Huang W (2012) Mechanical property and microstructural characterization of C–Mn–Al–Si hot dip galvanizing TRIP steel. J Iron Steel Res Int 19:29–36. https://doi.org/10.1016/S1006-706X(12)60136-8

[20] Wu ZQ, Ding H, An XH et al (2015) Influence of Al content on the strain-hardening behavior of aged low density Fe–

Mn–Al–C steels with high Al content. Mater Sci Eng A 639:187–191. https://doi.org/10.1016/j.msea.2015.05.002

[21] Yi HL, Lee KY, Bhadeshia HKDH (2011) Mechanical stabilisation of retained austenite in δ–TRIP Steel. Mater Sci Eng A 528:5900–5903

[22] Deng Z, Zhu M, Zhou Y, Sichen D (2016) Attachment of alumina on the wall of submerged entry nozzle during continuous casting of Al-killed steel. Metall Mater Trans B 47:2015–2025. https://doi.org/10.1007/s11663-016-0624-y

[23] Li Y, Ding W, Wang B (2019) Intercritical annealing pretreatment used in a hot-dip galvanised TRIP steel. Mater Sci Technol 35:1372–1380. https://doi.org/10.1080/02670836.2019.1625171

[24] Ding W, Hedström P, Li Y (2016) Heat treatment, microstructure and mechanical properties of a C–Mn–Al–P hot dip galvanizing TRIP steel. Mater Sci Eng A 674:151–157. https://doi.org/10.1016/j.msea.2016.07.119

[25] Ding W, Tang D, Jiang H, Huang W (2011) Influence of isothermal bainite transformation time on microstructure and mechanical properties of hot-dip galvanized TRIP steel. J Mater Eng Perform 20:997–1002. https://doi.org/10.1007/s11665-010-9714-1

[26] Sibley KD, Breyer NN (1976) The effect of silicon on the impact and tensile properties of low-carbon steels. Metall Trans A 7:1602–1604

[27] Jacques PJ, FurneÂmont Q, Mertens A, Delannay F (2001) On the sources of work hardening in multiphase steels assisted by transformation-induced plasticity. Philos Mag A 81:1789–1813

[28] Grässel O, Krüger L, Frommeyer G, Meyer LW (2000) High strength Fe–Mn–(Al, Si) TRIP/TWIP steels development—properties—application. Int J Plast 16:1391–1409

[29] Jeong K, Jin J-E, Jung Y-S et al (2013) The effects of Si on the mechanical twinning and strain hardening of Fe–18Mn–0.6 C twinning-induced plasticity steel. Acta Mater 61:3399–3410

[30] Sun B, Fazeli F, Scott C et al (2018) The influence of silicon additions on the deformation behavior of austenite-ferrite duplex medium manganese steels. Acta Mater 148:249–262. https://doi.org/10.1016/j.actamat.2018.02.005

[31] B.D.Cullity, S.R.Stock (2001) Elements of X-ray diffraction, 3rd edn

[32] Kang S, Speer JG, Krizan D et al (2016) Prediction of tensile properties of intercritically annealed Al-containing 0.19C-4.5Mn (wt%) TRIP steels. Mater Des 97:138–146. https://doi.org/10.1016/j.matdes.2016.02.058

[33] Koistinen DP, Marburger RE (1959) A general equation prescribing the extent of the austenite-martensite transformation in pure iron-carbon alloys and plain carbon steels. Acta Metall 7:59–60. https://doi.org/10.1016/0001-6160(59)90170-1

[34] Andrews KW (1965) Empirical formulae for the calculation of some transformation temperatures. J Iron Steel Inst 203:721–727

[35] Sugimoto K-I, Kobayashi M, Hashimoto S-I (1992) Ductility and strain-induced transformation in a high-strength transformation-induced plasticity-aided dual-phase steel. Metall Trans A 23:3085–3091

[36] Kang S, De Moor E, Speer JG (2015) Retained austenite stabilization through solute partitioning during intercritical annealing in C-, Mn-, Al-, Si-, and Cr-alloyed steels. Metall Mater Trans A 46:1005–1011. https://doi.org/10.1007/s11661-014-2708-0

[37] Chiang J, Lawrence B, Boyd JD, Pilkey AK (2011) Effect of microstructure on retained austenite stability and work hardening of TRIP steels. Mater Sci Eng A 528:4516–4521. https://doi.org/10.1016/J.MSEA.2011.02.032

[38] Timokhina IB, Hodgson PD, Pereloma EV (2004) Effect of microstructure on the stability of retained austenite in transformation-induced-plasticity steels. Metall Mater Trans A 35:2331–2341

[39] Lee S-J, Park K-S (2013) Prediction of martensite start temperature in alloy steels with different grain sizes. Metall Mater Trans A 44:3423–3427

[40] Sugimoto K, Misu M, Kobayashi M, Shirasawa H (1993) Effects of second phase morphology on retained austenite morphology and tensile properties in a trip-aided dual-phase steel sheet. ISIJ Int 33:775–782. https://doi.org/10.2355/isijinternational.33.775

[41] Lee S, Shin S, Kwon M et al (2017) Tensile Properties of Medium Mn Steel with a Bimodal UFG α + γ and Coarse δ - Ferrite Microstructure. Metall Mater Trans A 48:1678–1700. https://doi.org/10.1007/s11661-017-3979-z

[42] Ding W, Wang R, Li Y, Wang B (2020) High elongation of medium-manganese steel containing 1.0 wt.% Al after a short intercritical annealing time. J Mater Res Technol 9:7262–7272

[43] Rollett AD, Kocks UF (1993) A review of the stages of work hardening. In: Solid state phenomena, pp 1–18

[44] Shterner V, Timokhina IB, Beladi H (2016) On the work-hardening behaviour of a high manganese TWIP steel at different deformation temperatures. Mater Sci Eng A 669:437–446

[45] Püschl W (2002) Models for dislocation cross-slip in close-packed crystal structures: a critical review. Prog Mater Sci 47:415–461